Supporting Information for

Marine heatwave in the Bohai-Yellow Seas enhanced the July 2025 rainstorm in Beijing and its surrounding areas

Mengzhou Yang[1], Ning Zhao[2*], Shuya Wang[3], Shixue Li[4,5], Xiaohui Zhou[6], Yu-Xiang Qiao[7], and Er Lu[1]

[1]Qinghai Provincial Key Laboratory of Plateau Climate Change and Ecological Environment Effects / School of Ecology and Environmental Sciences, Qinghai Institute of Technology, Xining 810016, China.

[2]Research Institute for Global Change, Japan Agency for Marine-Earth Science and Technology, Yokosuka, 2370061, Japan.

[3]Advanced Institute for Marine Ecosystem Change (WPI-AIMEC), Tohoku University, Sendai, 9808578, Japan.

[4]School of Earth, Atmosphere, and Environment, Monash University, Clayton, VIC, Australia

[5]ARC Centre of Excellence for the Weather of the 21st Century, Monash University, Clayton, VIC, Australia.

[6]Earth System Science Interdisciplinary Center, University of Maryland, College Park, MD, U.S.

[7]Department of Geophysics, Graduate School of Science, Tohoku University, Sendai, Japan.

Brief introduction

This file contains a detailed explanation of our method in calculating contributions of different regions (Text S1 and Table S1) and the supplementary figures, including the locations/heights of particles at their release times (Figure S1), the standardized area-mean precipitation over Beijing and its surrounding areas (Figure S2), comparison of the large-scale circulations and moisture transport based on ERA5 and WRF simulation (Figure S3), comparison of surface latent heat fluxes and surface wind conditions in late July between the climatological mean and 2025 (Figure S4), temporal variations of rainfall-related particles in the BYS region and their mean arrival time from each grid to the BSA (Figure S5), statistics of particles released before and after 27 July 27 in the CTL run (Figures S6 and S7), comparison of latent heat fluxes between two WRF experiments (Figure S8), and statistics of cyclone-influenced and other particles based on different baseline radii (Table S2).

Text S1. An example iteration for the 'source attribution' method in Figure 4c

The general conception of our temporal contribution is: a) once moisture uptake is detected, its weighted contribution would be determined ($f(i,t)=\Delta Q(i,t)/Q(i,t)$), and all previous contributions will be diluted accordingly; and b) if precipitation is detected, all previously gained moisture will be reduced according to the weighted contributions. In simple terms, moisture uptake at previous times would be 'filtered' by precipitation that occurs later.

Here, an iteration example shows the general conception of our method. Considering a particle released at t=0 with unit mass, and its moisture content Q varied along its backward trajectory as shown in Table S1.

1) At t-4, the original moisture content of this particle was 10 (i.e., moisture uptake set to +10.0), and its fractional contribution was 1.0.
2) At t-3, the moisture uptake (+2.5) occurred, and the fractional contribution of original moisture content was reduced to 0.8 (=10.0/12.5), while the fractional contribution of the newer moisture uptake was 0.2 (=2.5/12.5).
3) At t-2, precipitation (-5.0) occurred. The moisture uptakes at t-4 and t-5 were reduced to 6.0 and 1.5, respectively, according to their fractional contributions (0.8 and 0.2).
4) At t-1, another moisture uptake occurred (+3.5), which further diluted the previous ones' contributions to 0.545 (=6.0/11.0) and 0.136(=1.5/11.0). The contribution of the newest uptake was 0.318 (=3.5/11.0).
5) At t=0, the final precipitation (-6.0) was detected. The fractional contributions of all uptakes remained unchanged, but the moisture gained at previous time steps were finally reduced to 2.727, 0.682, and 1.591, respectively.

Table S1. An iteration example for calculating temporal contributions. Q is the moisture content at each time step, ΔQ is the moisture changes, $\Delta Q_{filtered}$ is the filtered moisture content due to rainfall that occurs later, and f is the fractional contributions.

Time	$\boldsymbol{Q}$	$\boldsymbol{\Delta Q}$	$\boldsymbol{\Delta Q_{filtered}}$ t-4, t-3, t-2, t-1, t=0	$\boldsymbol{f}$ t-4, t-3, t-2, t-1, t=0
t=0	5.0	-6.0	n/a, n/a, n/a, n/a, n/a	n/a, n/a, n/a, n/a, n/a
t-1	11.0	+3.5	n/a, n/a, n/a, 3.5, 1.591	n/a, n/a, n/a, 0.318, 0.318
t-2	7.5	-5.0	n/a, n/a, n/a, n/a, n/a	n/a, n/a, n/a, n/a, n/a
t-3	12.5	+2.5	n/a, 2.50, 1.50, 1.50, 0.682	n/a, 0.2, 0.2, 0.136, 0.136
t-4	10.0	+10.0	10.0, 10.0, 6.0, 6.0, 2.727	1.0, 0.8, 0.8, 0.545, 0.545

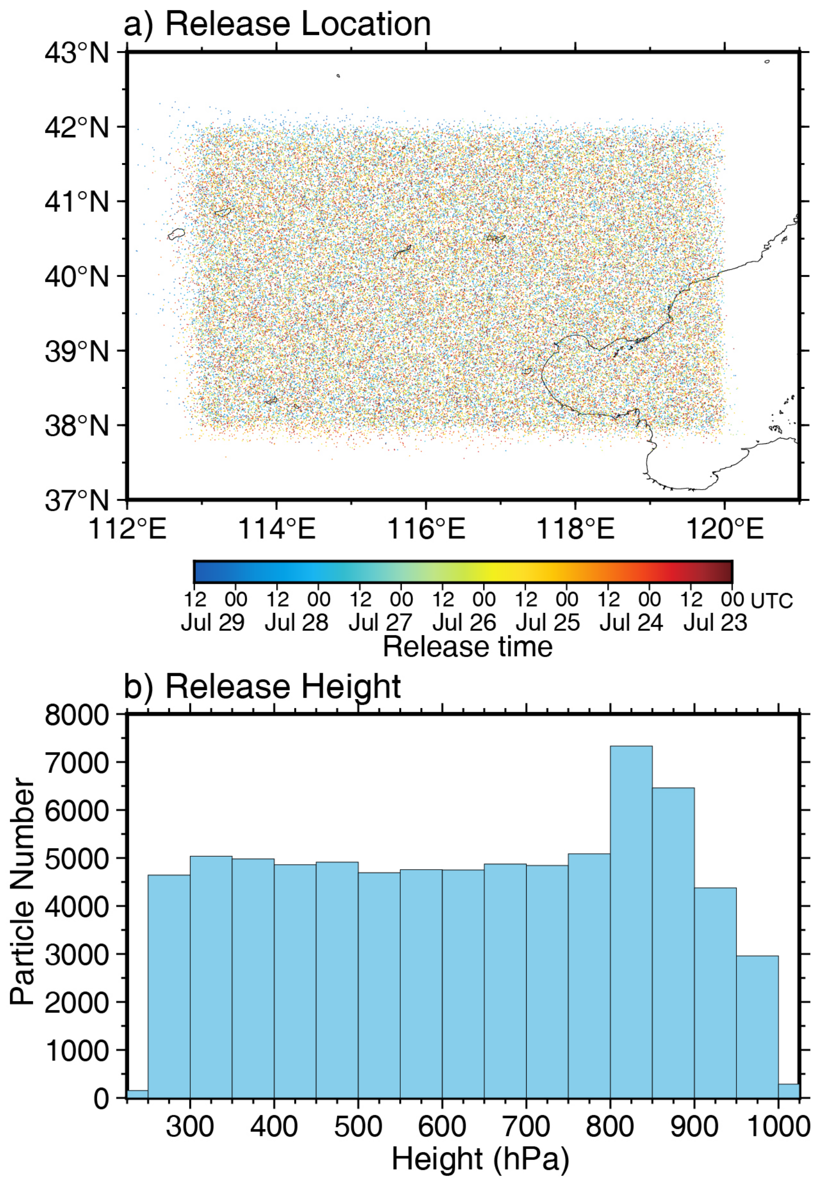

Figure S1. (a) Locations of the particles at their release times (color) and (b) a histogram of their heights. The relatively higher probability of particles around the 900-800 hPa levels was caused by the high-altitude regions north of Beijing (e.g., see topography in Figure 1a), as we released the particles from the surface, not the 1000-hPa level.

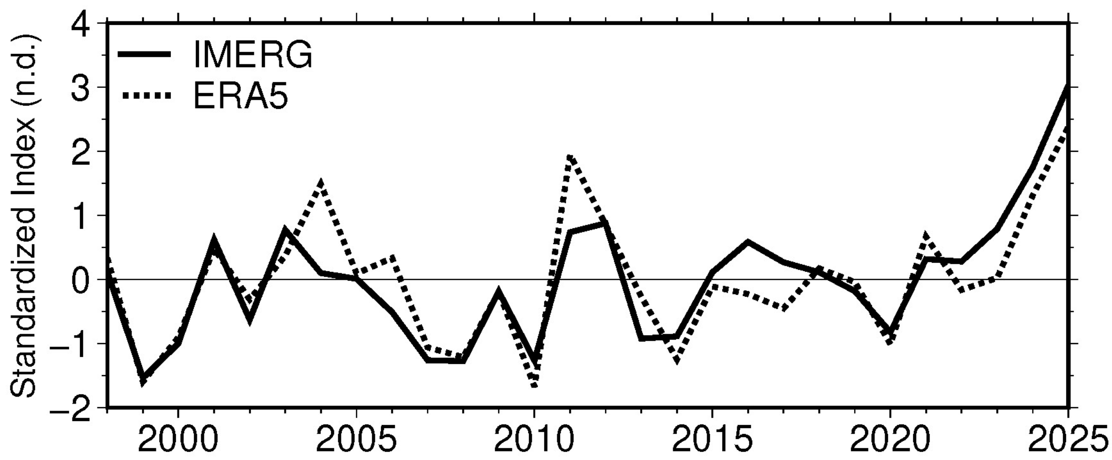

Figure S2. Time series of the standardized area-mean precipitation anomalies over Beijing and its surrounding areas (BSA) based on the satellite data IMERG and ERA5 from 1998 to 2025.

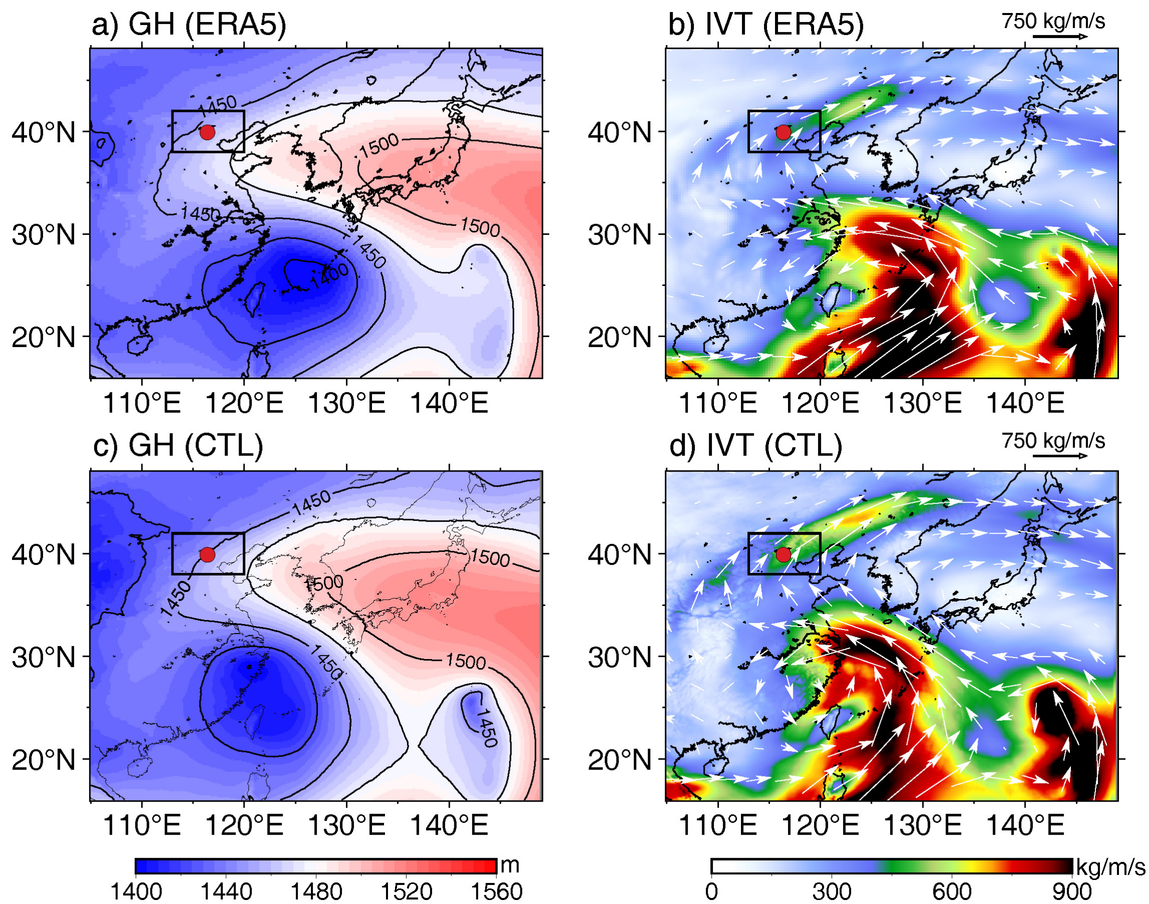

Figure S3. Comparison of (left) the mean geopotential height at 850-hPa level (GH; m) and (right) the vertically Integrated Vapor Transport (IVT; kg/m/s) based on (a and b) ERA5 and (c and d) the CTL run during the BSA rainstorm (00 UTC July 23 to 12 UTC July 29, 2025).

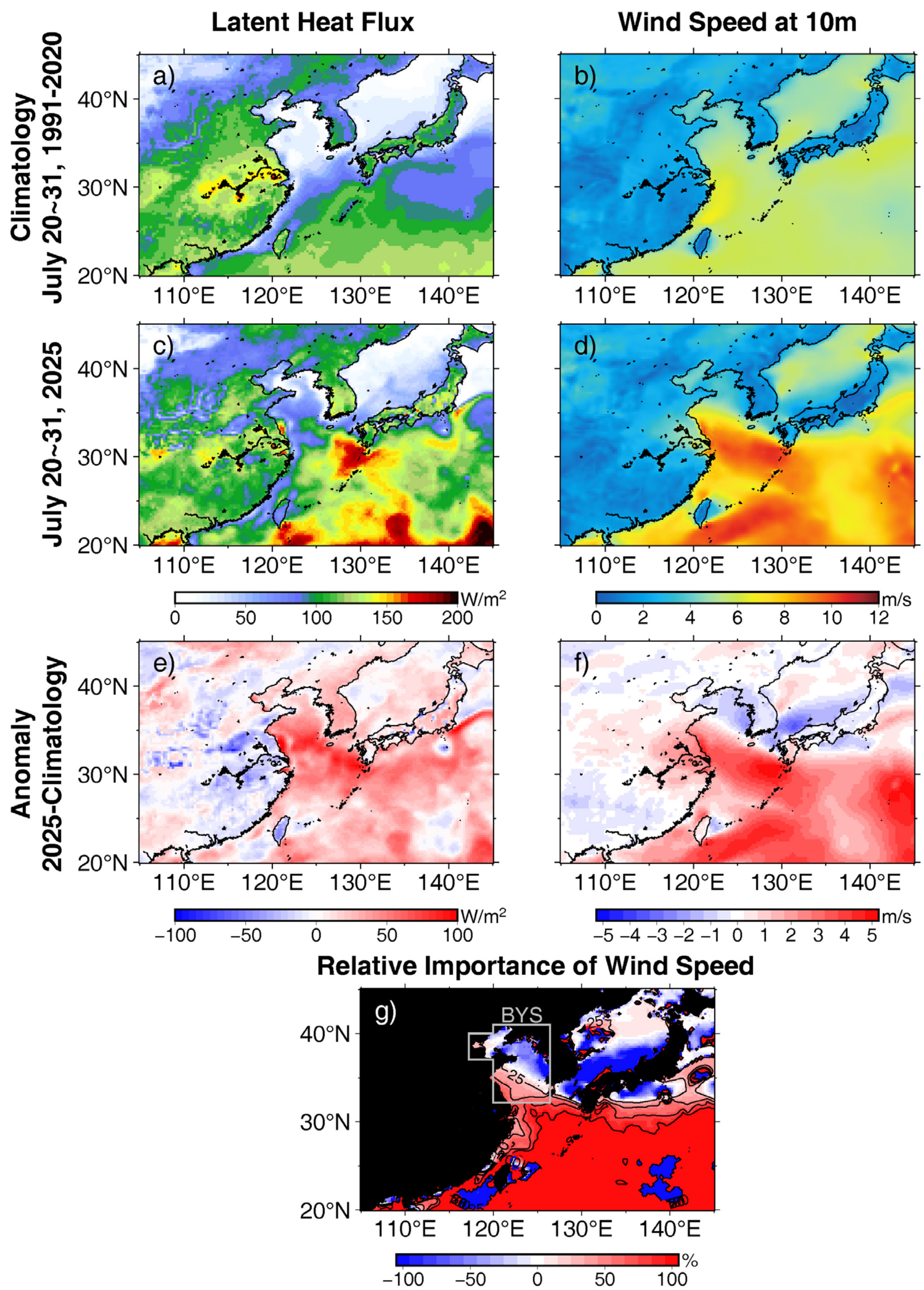

Figure S4. Comparison of (left) surface latent heat fluxes and (right) surface wind conditions in late July (July 20~31) based on ERA5: (a, b) the climatological mean during the baseline period of 1991~2020, (c, d) period mean in 2025, and (e, f) their differences (2025 minus Climatology). The relative importance of wind speed in panel g was estimated by $\frac{\Delta W_{10_{2025-CLIM}}}{W_{10_{CLIM}}} / \frac{\Delta LH_{2025-CLIM}}{LH_{CLIM}}$ by assuming other factors in latent heat flux remained unchanged (i.e., $\boldsymbol{\Delta LH \propto \Delta W_{10}}$).

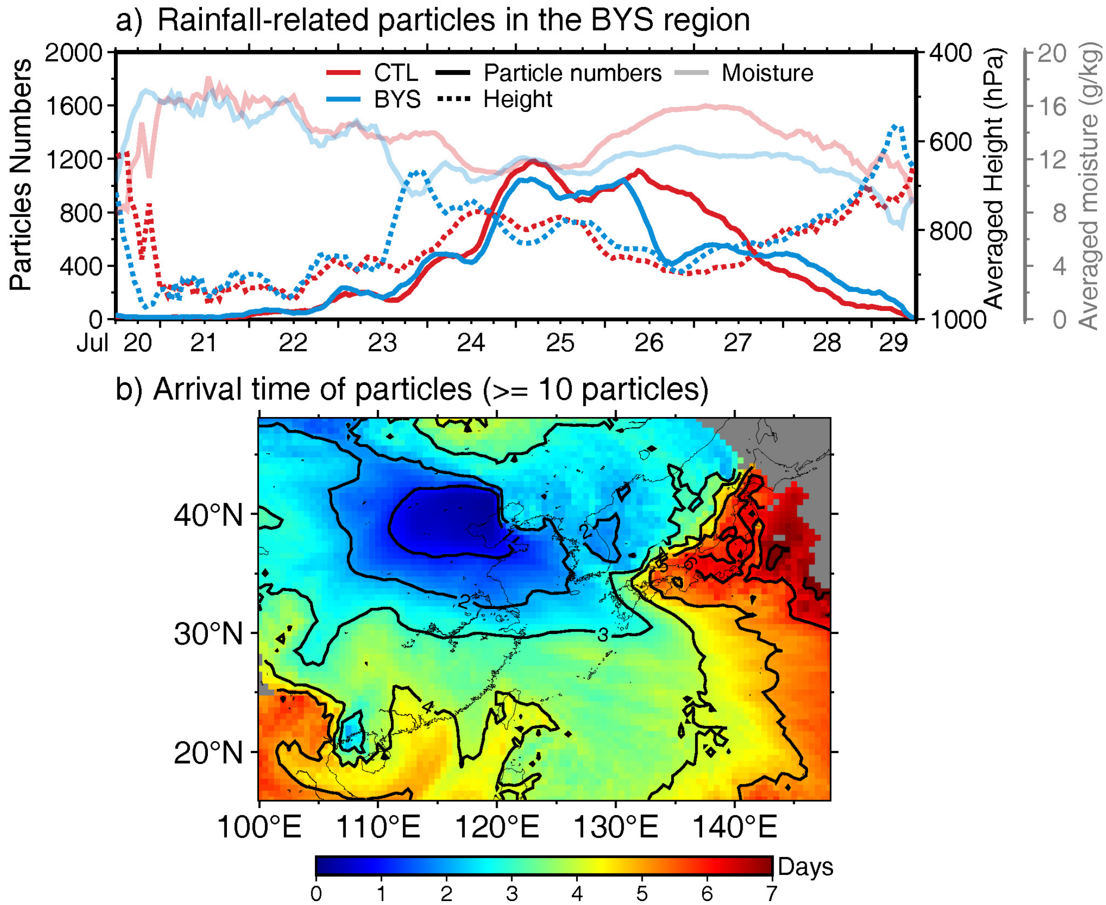

Figure S5. (a) Time series of the number of rainfall-related particles (solid lines) and their mean height (dashed lines), and moisture content (gray lines) based on CTL and BYS runs, and (b) the mean arrival time of particles to the BSA depending on their locations (only plotted when more than 10 particles passed).

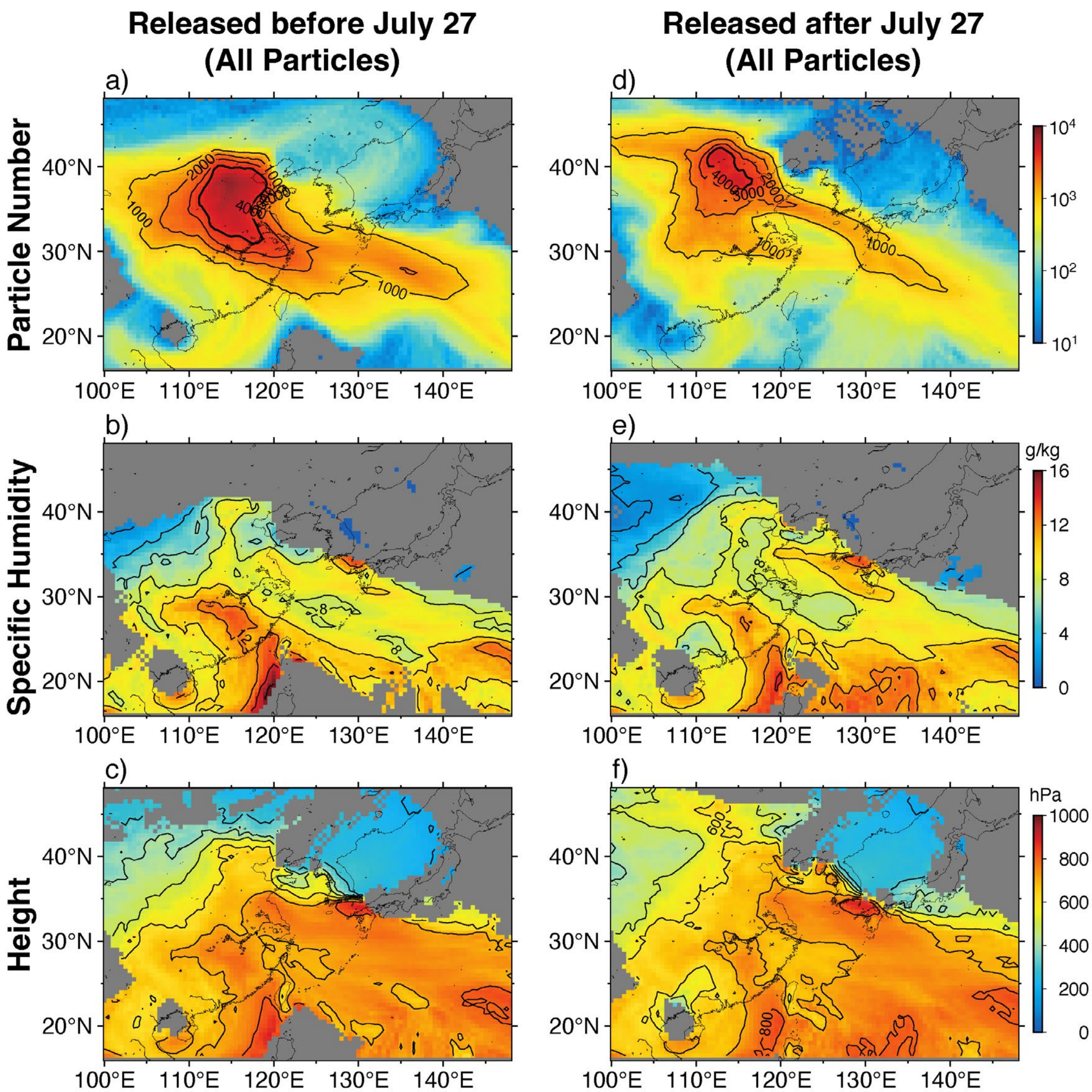

Figure S6. Same as Figure 3 but for particles released before and after 27 July 27 in the CTL run, including (a, b) particle numbers and their (c, d) mean specific humidity, and (e, f) mean height. Only grids passed by more than 10 particles were plotted.

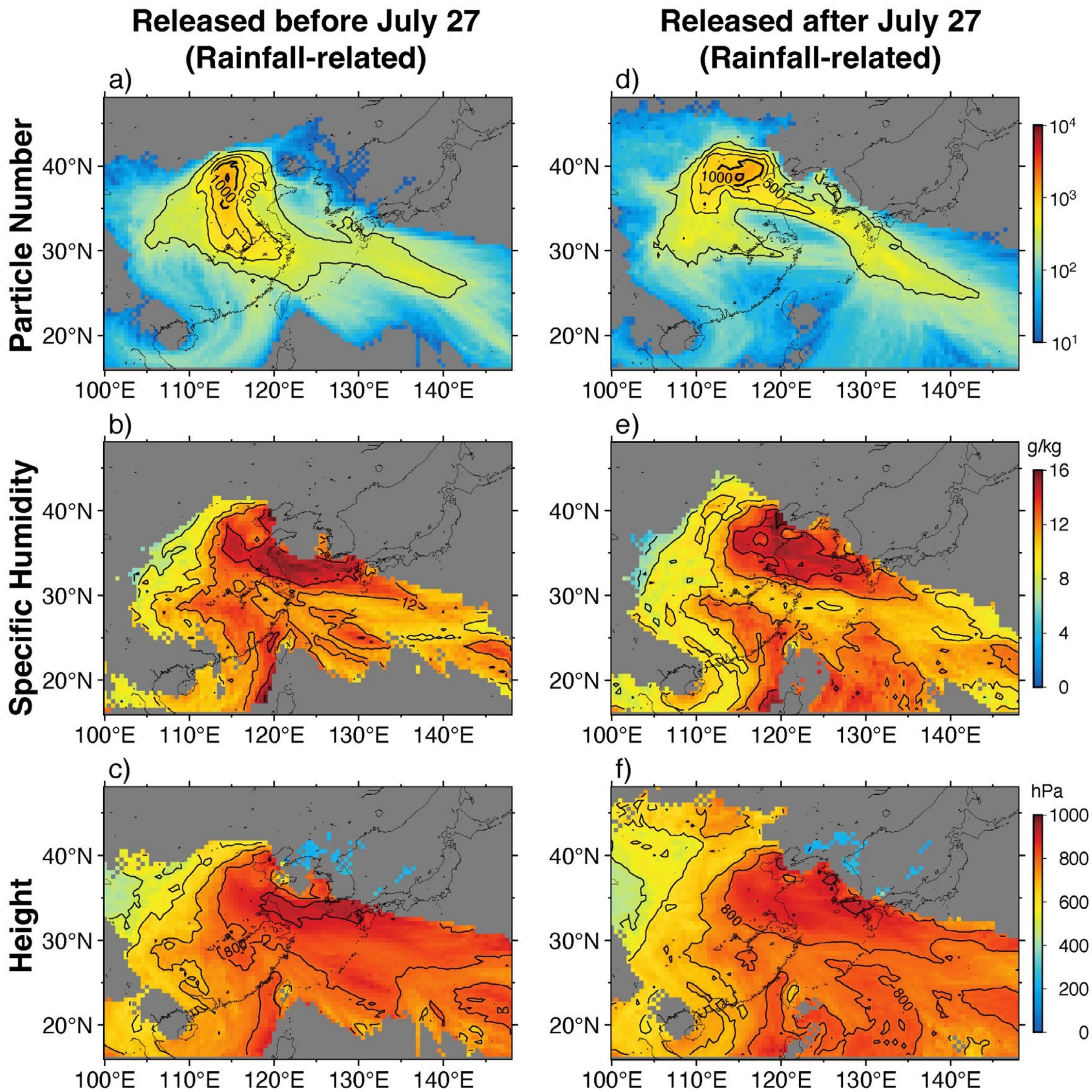

Figure S7. Same as Figure S6 but for rainfall-related particles.

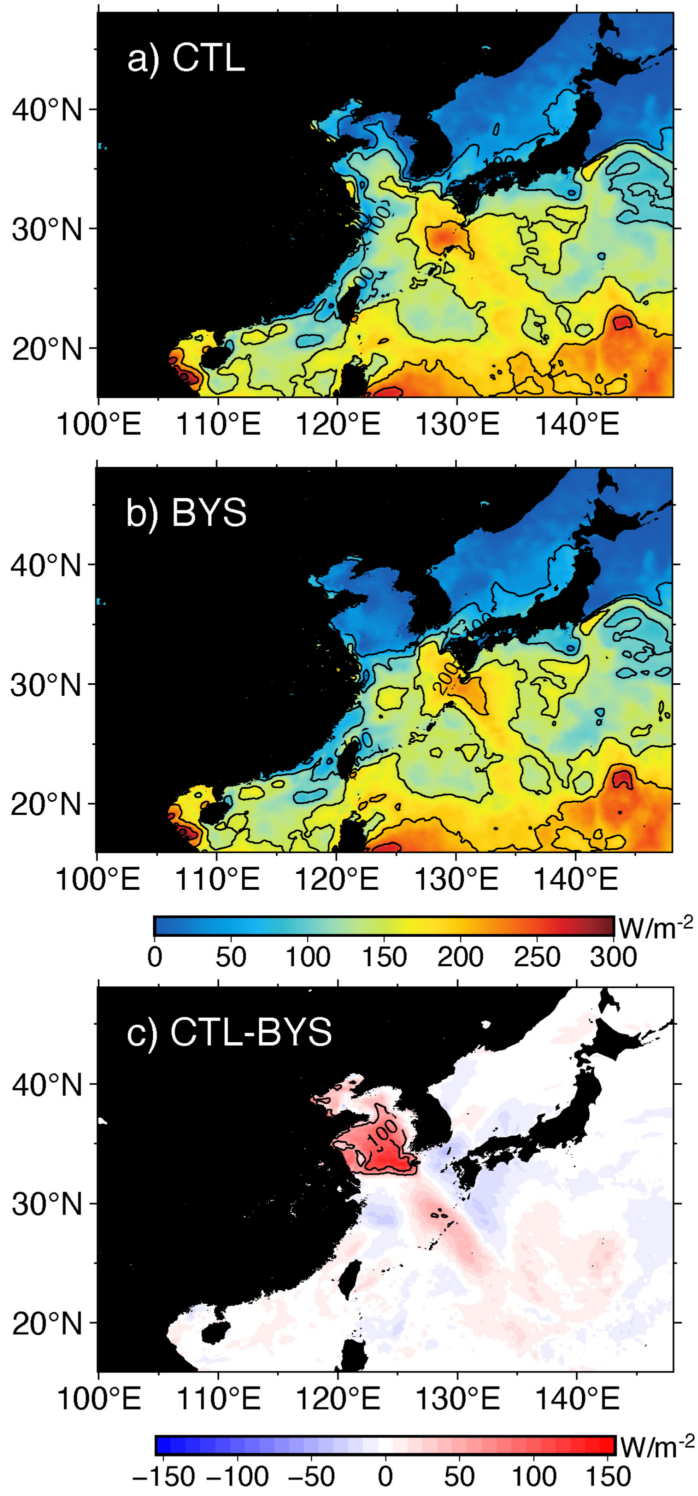

Figure S8. Comparison of sea surface latent heat fluxes between two numerical experiments averaged over the simulation period (July 20~30): a) CTL run, b) BYS run, and c) their difference.

Table S2. Statistics of cyclone-influenced and other particles based on different baseline radii among 12,922 rainfall-related and all 75,000 particles.

Rainfall-related particles **Baseline Radius**	**Wipha**	**Francisco**	**Co-May**	**Krosa**	**Other**
600 km	2971 (22.99%)	3509 (27.16%)	500 (3.87%)	55 (0.43%)	6124
700 km	3004 (23.25%)	3512 (27.18%)	579 (4.48%)	162 (1.25%)	5990
800 km	3030 (23.45%)	3519 (27.23%)	660 (5.11%)	268 (2.07%)	5855
900 km	3101 (24.00%)	3549 (27.46%)	742 (5.74%)	439 (3.40%)	5660
1000 km	3237 (25.05%)	3989 (30.87%)	876 (6.78%)	649 (5.02%)	5071
All particles	**Wipha**	**Francisco**	**Co-May**	**Krosa**	**Other**
600 km	10716 (14.29%)	13342 (17.79%)	1651 (2.20%)	191 (0.25%)	50025
700 km	10853 (14.47%)	13351 (17.80%)	2040 (2.72%)	473 (0.63%)	49566
800 km	10926 (14.57%)	13375 (17.83%)	2469 (3.29%)	823 (1.10%)	49133
900 km	11275 (15.03%)	13492 (17.99%)	2807 (3.74%)	1374 (1.83%)	48373
1000 km	12101 (16.13%)	15358 (20.48%)	3313 (4.42%)	2019 (2.69%)	45772